

## Evaluation of supersingular integrals: Second-order boundary derivatives<sup>‡</sup>

M. N. J. Moore<sup>1,2</sup>, L. J. Gray<sup>1,\*</sup>,<sup>†</sup> and T. Kaplan<sup>1</sup>

<sup>1</sup>*Computer Science and Mathematics Division, Oak Ridge National Laboratory, Oak Ridge, TN 37831, U.S.A.*

<sup>2</sup>*Department of Mathematics, University of North Carolina, Chapel Hill, NC 27599, U.S.A.*

### SUMMARY

The boundary integral representation of second-order derivatives of the primary function involves second-order (hypersingular) and third-order (supersingular) derivatives of the Green's function. By defining these highly singular integrals as a difference of boundary limits, interior minus exterior, the limiting values are shown to exist. With a Galerkin formulation, coincident and edge-adjacent supersingular integrals are separately divergent, but the sum is finite, while the individual hypersingular integrals are finite. Moreover, the cancellation of the supersingular divergent terms only requires a continuous interpolation of the surface potential, and there is no continuity requirement on the surface flux. The algorithm is efficient, the non-singular integrals vanish and the singular integrals are computed entirely analytically, and accurate values are obtained for smooth surfaces. However, it is shown that a (continuous) linear interpolation is not appropriate for evaluation at boundary corners. Published in 2006 by John Wiley & Sons, Ltd.

Received 3 March 2006; Revised 6 June 2006; Accepted 12 June 2006

KEY WORDS: boundary integral method; surface derivatives; supersingular integrals; boundary limit

### 1. INTRODUCTION

The result of a standard boundary integral equation analysis is that the primary function, e.g. potential in a Laplace problem or displacement in elasticity, and the 'normal derivative', surface flux or surface traction, respectively, are known everywhere on the boundary [1, 2]. In many cases

\*Correspondence to: L. J. Gray, Computer Science and Mathematics Division, ORNL, Oak Ridge, TN 37831, U.S.A.

<sup>†</sup>E-mail: ljg@ornl.gov

<sup>‡</sup>This article is a U.S. Government work and is in the public domain in the U.S.A.

Contract/grant sponsor: Office of Mathematical, Information, and Computational Sciences, U.S. Department of Energy; contract grant number: DE-AC05-00OR22725

Contract/grant sponsor: Oak Ridge National Laboratory

Contract/grant sponsor: Spanish Ministry of Education, Culture and Sport; contract/grant number: SAB2003-0088

however, it is necessary to use this information to obtain, in a post-processing step, all first-order derivatives on the boundary, e.g. the potential gradient or stress tensor. Adopting, for concreteness, the language and notation of the two-dimensional Laplace equation  $\nabla^2\phi=0$  for the potential  $\phi$ , the boundary integral expression for the gradient of  $\phi$  can be written as

$$\nabla_P\phi(P) = \int_{\Gamma} \left( \frac{\partial\phi}{\partial\mathbf{n}}(Q)\nabla_P G(P, Q) - \phi(Q)\nabla_P \frac{\partial G}{\partial\mathbf{n}}(P, Q) \right) d\Gamma_Q \quad (1)$$

This equation will be (modified and) defined more carefully in the next section, but for now we simply note that the evaluation of the hypersingular integral involving two derivatives of the Green's function

$$G(P, Q) = -\frac{1}{2\pi} \log(\|Q - P\|) = -\frac{1}{2\pi} \log(r) \quad (2)$$

has been somewhat problematic, especially for collocation approximations [3, 4]. As a consequence, a variety of methods for gradient evaluation have been proposed, roughly characterized as: (a) direct evaluation of Equation (1) [5–7]; (b) reformulation of Equation (1) to remove the hypersingularity [8, 9]; and (c) methods not based on an integral representation [10, 11]. Please see References [12, 13] for a more complete discussion and additional references to the extensive literature.

The impetus for the work herein is the successful analysis of Equation (1) based upon defining the integrals as the difference of interior and exterior boundary limits [5, 14] (again, to be defined more precisely below). An important observation emerging from this work is that, in this interior/exterior boundary limit scheme, the gradient hypersingular integral in Equation (1) does not exhibit what might be called typical hypersingular behaviour. In a Galerkin implementation of the ‘standard’ hypersingular integral, namely the normal derivative hypersingular equation with the limit taken from either the exterior or interior, both coincident and adjacent singular integrals are separately divergent. However, assuming the potential is continuous ( $\mathcal{C}^0$ ) on the boundary, the complete integral is finite, the divergent terms from the individual element integrals cancel [15, 16] (for collocation,  $\mathcal{C}^1$  is required for the existence of the integral [3]). It is this divergent term behaviour that is not seen in the gradient analysis, all element integrals are finite: potentially divergent terms are the same on either side of the boundary and simply cancel in the difference of the limits. Said another way, contrary to the experience with the normal derivative hypersingular integral, the gradient hypersingular integral exists without any inter-element continuity requirement on the potential  $\phi$ .

The ‘interior/exterior limit’ gradient algorithm therefore effectively reduces the severity of the kernel singularities by one order, and the continuity requirements are weakened. Based upon this, there is good reason to expect that, with a simple  $\mathcal{C}^0$  interpolation, limit-differenced Galerkin integrals of third-order derivatives of  $G(P, Q)$  could be finite. The main result of this paper is that this is indeed the case, and that as a consequence, second-order derivatives of  $\phi$  can be computed. For a smooth surface, a  $\mathcal{C}^0$  interpolation will suffice for the evaluation of these derivatives. However, a low-order interpolation will not produce accurate second derivatives at a boundary corner, despite the fact that the boundary integrals are finite.

Adopting the terminology of Reference [17], the third-order derivative of the Green's function will be called *supersingular*. It is expected that the divergent term behaviour of Galerkin supersingular integrals will be similar to the (manageable) normal derivative hypersingular: the separate coincident and adjacent element integrals are divergent, but the sum of all integrals is finite. This will be established, for simplicity and convenience, taking the two-dimensional Laplace equation

and a linear interpolation as the setting. The limit techniques apply directly to other Green's functions and, based upon the previous gradient analysis in three dimensions, will likely extend more or less directly for the higher dimension as well.

Boundary integral equations having kernel functions beyond hypersingular have not been extensively studied, References [17–20] may in fact be the entire literature on the subject. The most advanced work is the recent paper by Frangi and Guiggiani [19], which provides a detailed analysis in the context of Kirchoff plate theory, and confirming numerical evaluations. The work in Reference [19], as herein, is based upon a direct analysis of the singular integrals, i.e. explicit calculation of the divergent terms and demonstration of cancellation. However, the limit process employed therein is reminiscent of (but not the same as) a 'Cauchy Principal Value' exclusion zone approach [21, 22], and is therefore significantly different from the boundary limits employed in this paper. Moreover, Reference [19] uses collocation, and thus the continuity requirement in their analysis for the existence of the supersingular integral is  $\mathcal{C}^2$ . The other significant difference is computational effort: a complete boundary integration is necessarily employed, whereas only singular integrals need to be considered for the interior/exterior boundary limit method.

In addition to the gradient methods mentioned above, it should be noted that a method for computing *all* higher order derivatives, without hypersingular or supersingular integrands, was presented by Schwab and Wendland [23]. In this bootstrapping procedure,  $(n + 1)$ th order derivatives are computed from  $n$ th order by solving a succession of boundary integral problems, all with the same coefficient matrix (stemming from standard boundary integral kernels); however, new right-hand side vectors must be computed at each stage, once again necessitating a complete boundary integration.

Second-order derivatives are known to be useful for plate analyses [19], and for the evaluation of  $\phi$  at interior points close to the boundary [23]. It is hoped that the ability to accurately compute these derivatives, without the expense of a complete boundary integration, will lead to their use in other contexts. One immediate application is the development of a *complete* cubic Hermite interpolation. As first proposed by Watson [24], the Hermite element directly incorporates gradient information into the interpolation of the primary function (e.g. potential  $\phi$ ) [25]. However, to extend this interpolation to the boundary flux, second-order derivatives are obviously necessary. Moreover, it is hoped that applications that require a non-linear iteration, such as contact problems [26] or shape optimization [27], can effectively exploit the availability of this higher order derivative information.

## 2. BOUNDARY INTEGRAL REPRESENTATIONS

The boundary integral equation for surface potential can be written as either an interior or exterior boundary limit:

$$\begin{aligned} \phi(P) + \lim_{\varepsilon \rightarrow 0^-} \int_{\Gamma} \left[ \phi(Q) \frac{\partial G}{\partial \mathbf{n}}(P_{\varepsilon}, Q) - G(P_{\varepsilon}, Q) \frac{\partial \phi}{\partial \mathbf{n}}(Q) \right] dQ &= 0 \\ \lim_{\varepsilon \rightarrow 0^+} \int_{\Gamma} \left[ \phi(Q) \frac{\partial G}{\partial \mathbf{n}}(P_{\varepsilon}, Q) - G(P_{\varepsilon}, Q) \frac{\partial \phi}{\partial \mathbf{n}}(Q) \right] dQ &= 0 \end{aligned} \quad (3)$$

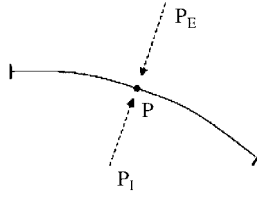


Figure 1. Illustration of the limit procedure at the boundary point  $P$ , the difference of the interior  $P_I$  and exterior  $P_E$  limits will be computed.

where  $G(P, Q)$  is defined in Equation (2),  $P$  is a boundary point and  $P_\varepsilon = P + \varepsilon\mathbf{N}$ ,  $\mathbf{N} = \mathbf{N}(P)$  the unit outward normal at  $P = (x_p, y_p)$ . Thus,  $\varepsilon > 0$  is an exterior limit and  $\varepsilon < 0$  is interior. With  $P_\varepsilon$  off the boundary, the kernel functions in Equation (3) are not singular and these two equations can be differentiated by moving the derivative under the integral sign. Taking the difference, interior minus exterior, Equation (1) can be replaced by [5]

$$\begin{aligned} \nabla_P \phi(P) &= \lim_{\varepsilon \rightarrow 0^-} \int_{\Gamma} \left( \frac{\partial \phi}{\partial \mathbf{n}}(Q) \nabla_P G(P_\varepsilon, Q) - \phi(Q) \nabla_P \frac{\partial G}{\partial \mathbf{n}}(P_\varepsilon, Q) \right) d\Gamma_Q \\ &\quad - \lim_{\varepsilon \rightarrow 0^+} \int_{\Gamma} \left( \frac{\partial \phi}{\partial \mathbf{n}}(Q) \nabla_P G(P_\varepsilon, Q) - \phi(Q) \nabla_P \frac{\partial G}{\partial \mathbf{n}}(P_\varepsilon, Q) \right) d\Gamma_Q \end{aligned} \quad (4)$$

This process is illustrated in Figure 1,  $P_E$  and  $P_I$ , respectively, denoting exterior and interior limit points approaching the boundary point  $P$ . The immediate advantage of this procedure is that as all non-singular integrals are independent of  $\varepsilon$ , they vanish. Carrying this process one step further, a general second-order derivative can be written (if the limits exist) as, simplifying the notation,

$$\begin{aligned} \frac{\partial^2}{\partial \mathcal{X} \partial \mathcal{Y}} \phi(P) &= \left\{ \lim_{\varepsilon \rightarrow 0^-} - \lim_{\varepsilon \rightarrow 0^+} \right\} \\ &\quad \times \int_{\Gamma} \left( \frac{\partial \phi}{\partial \mathbf{n}}(Q) \frac{\partial^2 G}{\partial \mathcal{X} \partial \mathcal{Y}}(P_\varepsilon, Q) - \phi(Q) \frac{\partial^3 G}{\partial \mathcal{X} \partial \mathcal{Y} \partial \mathbf{n}}(P_\varepsilon, Q) \right) d\Gamma_Q \end{aligned} \quad (5)$$

where  $\mathcal{X}$  and  $\mathcal{Y}$  denote either  $x_p$  or  $y_p$ . Formulas for the derivatives of  $G$  are easily obtained from Equation (2), and are relegated to Appendix A.

In the gradient evaluation in References [5, 14] for three and two dimensions, respectively, the details of the limit analysis for the hypersingular kernel have been presented. Thus the next section will only consider the supersingular third-order derivative of  $G$ . First, however, we set notation by briefly reviewing the linear element Galerkin approximation.

### 2.1. Galerkin approximation

The simplest possible continuous interpolation in two dimensions is linear. A boundary element is defined by two nodes  $Q_j = (x_j, y_j)$ ,  $j = 1, 2$ , and the linear interpolation of the boundary is then

$$Q(t) = (x(t), y(t)) = \sum_{j=1}^2 (x_j, y_j) \psi_j(t) \quad (6)$$

## SECOND-ORDER DERIVATIVES

with shape functions  $\psi_j(t)$ ,  $t \in [0, 1]$ ,

$$\begin{aligned}\psi_1(t) &= 1 - t \\ \psi_2(t) &= t\end{aligned}\tag{7}$$

The corresponding interpolation of the surface potential is

$$\phi(Q(t)) = \sum_{j=1}^2 \phi(Q_j) \psi_j(t)\tag{8}$$

and similarly for the flux.

In addition to defining the boundary and function interpolations, the shape functions are also employed as the weight functions in the Galerkin formulation. Dropping the dependence on  $\varepsilon$  and the boundary limits (henceforth understood), the Galerkin form of Equation (5) is

$$\begin{aligned}\int_{\Gamma} \psi_k(P) \frac{\partial^2}{\partial \mathcal{X} \partial \mathcal{Y}} \phi(P) \, d\Gamma_P \\ = \int_{\Gamma} \psi_k(P) \int_{\Gamma} \left( \frac{\partial \phi}{\partial \mathbf{n}}(Q) \frac{\partial^2 G}{\partial \mathcal{X} \partial \mathcal{Y}}(P, Q) - \phi(Q) \frac{\partial^3 G}{\partial \mathcal{X} \partial \mathcal{Y} \partial \mathbf{n}}(P, Q) \right) \, d\Gamma_Q \, d\Gamma_P\end{aligned}\tag{9}$$

where the weight function  $\psi_k(P)$  is comprised of the two shape functions that are non-zero at a particular node  $P_k$ . As in References [16, 28], this equation results in a system of linear equations for the derivative values everywhere on the boundary. The coefficient matrix, originating from the integral on the left is quite simple: the matrix elements are comprised of integrals of pairs of shape functions, resulting in a sparse, symmetric positive definite system. This matrix is the same as that for the gradient calculation, and thus also the same for all three second-order derivatives. As only the right-hand side changes, only one LU factorization is required. For large-scale problems however, an iterative solver exploiting the sparsity and positive definiteness would likely be more effective.

Note that even at a boundary corner, the Galerkin weight function is comprised of two shape functions, i.e. the weight function spans both sides of the corner. Unlike the flux, the derivatives are (assumed to be) continuous functions on the domain, and thus for derivative evaluation, the Galerkin corner treatment discussed in Reference [29] is not required.

Nevertheless, boundary corners are generally more difficult than smooth surface points, and not surprisingly this is also the case for second derivative evaluation. Note that *if* continuity were required for evaluating the hypersingular integral in the above equation, then calculating second-order derivatives at boundary corners would be impossible: the flux is inherently discontinuous at a boundary corner due to the change in normal vector. As noted above, within a Galerkin approximation, this flux integral exists without any inter-element continuity constraint and is therefore not a problem. On the other hand, the supersingular integral will prove to be difficult at a corner. Even though the boundary limit will exist, it will be demonstrated below that a linear interpolation cannot produce an accurate corner solution.

In the discretization of Equation (9), the boundary integrations are carried out as a sum over elements, and thus an integration is required for every pair of elements  $\{E_P, E_Q\}$ . However, if

the difference of the limits is taken, only singular terms can contribute to the integral, reducing considerably the computational work. It is therefore only necessary to integrate over coincident ( $E_P = E_Q$ ) or adjacent pairs ( $E_P$  and  $E_Q$  share a node). The next section considers these two cases separately.

### 3. LIMIT ANALYSIS

As discussed above, it is expected that the limit-difference behaviour of the supersingular integral is analogous to a (one-sided limit) hypersingular integral. Thus, the coincident and adjacent singular integrals will be found to be separately divergent, but the complete integral will be finite. The primary difference is that the divergent term for the one-sided hypersingular integral is of the form  $\log(\varepsilon^2)$ , whereas here, not surprisingly, it will turn out to be one step further down,  $\varepsilon^{-1}$ .

For purposes of discussion, it suffices to examine the second derivative with respect to  $x_P$ , as the two remaining cases are handled identically. The coincident integral, although more singular, is actually the easier of the two and is examined first.

#### 3.1. Coincident integration

Replacing the potential by its approximation in terms of shape functions, the coincident,  $E_P = E_Q = E$ , integrals to be evaluated are then

$$\phi(Q_j) \int_E \psi_k(P) \int_E \psi_j(Q) \frac{\partial^3 G(P, Q)}{\partial x_P^2 \partial \mathbf{n}} dQ dP \tag{10}$$

The kernel function is

$$\frac{\partial^3 G(P, Q)}{\partial x_P^2 \partial \mathbf{n}} = -\frac{1}{2\pi} \left( \frac{-6n_x R_1 - 2n_y R_2}{r^4} + \frac{8R_1^2 (\mathbf{n} \cdot \mathbf{R})}{r^6} \right) \tag{11}$$

where  $\mathbf{R} = Q - P$ ,  $r = \|\mathbf{R}\|$ ,  $\mathbf{n}(Q) = (n_x, n_y)$  the unit outward normal at  $Q$ . The parameter for the  $Q$  integration will be denoted by  $s \in [0, 1]$ , and  $t$  the corresponding parameter for  $P$ . The element  $E = [P_1, P_2]$  is defined by the two nodes  $P_1 = (x_1, y_1)$  and  $P_2 = (x_2, y_2)$ , with  $s = 0$  corresponding to  $P_1$ .

As the singularity is at  $s = t$ , the first step in the  $Q$  integration is a change of variables,  $u = s - t$ , the singularity now located at  $u = 0$ . The distance function is then a simple quadratic polynomial

$$\frac{1}{r^2} = \frac{1}{\varepsilon^2 + a^2 u^2} \tag{12}$$

where  $a^2 = a_x^2 + a_y^2$ ,  $a_x = x_2 - x_1$ ,  $a_y = y_2 - y_1$ . Thus, there is no problem in the analytic integration, with respect to  $\{u, t\}$ , of these simple rational functions. (The tedious integration and limit analysis

## SECOND-ORDER DERIVATIVES

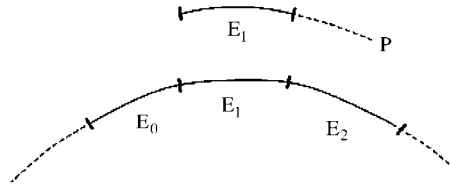


Figure 2. For the outer  $P$  integration over an element  $E_1$  there are three singular integrals, the coincident and two adjacent. The divergences in the integrals are associated with the endpoints and will cancel.

can be easily automated using a symbolic computation program.) The results are perhaps a bit surprising, there is no finite contribution from this coincident integral Equation (10), only the divergent terms remain,

$$\begin{aligned}\mathcal{S}_{11}^{XX} &= -\phi(P_1) \frac{1}{\varepsilon} \frac{a_y^2 - a_x^2}{\pi a^2} \\ \mathcal{S}_{22}^{XX} &= -\phi(P_2) \frac{1}{\varepsilon} \frac{a_y^2 - a_x^2}{\pi a^2}\end{aligned}\quad (13)$$

The subscripts here refer to the indices  $k, j$  associated with the  $P$  and  $Q$  shape functions, and all other terms not shown are zero. The superscript  $XX$  indicates that these are the results for the second derivative with respect to  $X$ . The corresponding formulas for the other two derivatives are:

$$\begin{aligned}\mathcal{S}_{11}^{XY} &= 2\phi(P_1) \frac{1}{\varepsilon} \frac{a_y a_x}{\pi a^2} \\ \mathcal{S}_{22}^{XY} &= 2\phi(P_2) \frac{1}{\varepsilon} \frac{a_y a_x}{\pi a^2} \\ \mathcal{S}_{11}^{YY} &= \phi(P_1) \frac{1}{\varepsilon} \frac{a_y^2 - a_x^2}{\pi a^2} \\ \mathcal{S}_{22}^{YY} &= \phi(P_2) \frac{1}{\varepsilon} \frac{a_y^2 - a_x^2}{\pi a^2}\end{aligned}\quad (14)$$

Thus, as expected, there is a divergent term associated with each endpoint of the element, and these will cancel with the corresponding adjacent integrations on either side. This is illustrated schematically in Figure 2: the Galerkin coincident integral over the element  $E_1$  produces divergent terms (associated with its endpoints) that will be shown to cancel with the adjacent-singular integrals over the pairs  $[E_1, E_0]$  and  $[E_1, E_2]$ .

For the flux integral in Equation (9), a complete analytic integration is easily carried out, resulting in no divergent terms (analogous to the hypersingular integral in gradient evaluation),

and finite quantities

$$\begin{aligned} \mathcal{J}_{12}^{XX} &= -\frac{a_x a_y}{a^2}, & \mathcal{J}_{21}^{XX} &= \frac{a_x a_y}{a^2} \\ \mathcal{J}_{12}^{XY} &= \frac{a_x^2 - a_y^2}{2a^2}, & \mathcal{J}_{21}^{XY} &= \frac{a_y^2 - a_x^2}{2a^2} \\ \mathcal{J}_{12}^{YY} &= \frac{a_x a_y}{a^2}, & \mathcal{J}_{21}^{YY} &= -\frac{a_x a_y}{a^2} \end{aligned} \tag{15}$$

all diagonal contributions  $k = j$  being zero.

### 3.2. Adjacent integration

As just noted, there are two cases to consider, one in which the  $Q$  element  $E_Q$  precedes  $E_P$ , as defined by the boundary orientation, and  $E_Q$  following  $E_P$ . There is however little difference in the way the calculations are handled, and thus it suffices to consider the inner  $Q$  integration to be over the preceding element  $E_Q = [P_0, P_1]$ ,  $P_0 = (x_0, y_0)$ ,  $E_P = [P_1, P_2]$  as above. At the shared node  $P_1$  we expect to find a divergent term multiplying  $\phi(P_1)$  that cancels with Equation (13); of course this cancellation would not occur if the interpolation of  $\phi$  were not continuous at  $P_1$ . The same analysis will apply when  $E_P$  precedes  $E_Q$ , the divergence now multiplied by  $\phi(P_2)$ .

The integral to be evaluated is

$$\phi(Q_j) \int_{E_P} \psi_k(P) \int_{E_Q} \psi_j(Q) \frac{\partial^3 G(P_\varepsilon, Q)}{\partial x_p^2 \partial \mathbf{n}} dQ dP \tag{16}$$

and again the difference of interior and exterior boundary limits is understood. The divergent term will come from  $k = 1$  and  $j = 2$ , the shape functions that are non-zero at  $P_1$ ; all other combinations of shape functions introduce an additional zero in the integrand at the singular point  $P_1$ , and this is sufficient for the integrals to have finite limits.

As in the previous section,  $Q$  is parameterized by  $s \in [0, 1]$  and  $P$  by  $t \in [0, 1]$ . The singularity is therefore located at  $(s, t) = (1, 0)$ , and a change of variables  $w = 1 - s$  is employed to move the singularity to  $(w, t) = (0, 0)$ , and the  $(w, t)$  domain remaining the unit square. As in Reference [15], it is now convenient to introduce polar co-ordinates

$$\begin{aligned} w &= \rho \cos(\theta) \\ t &= \rho \sin(\theta) \end{aligned} \tag{17}$$

so that the integral in Equation (16), omitting for now the  $\phi(Q_j)$  factor, can be expressed as

$$\begin{aligned} \int_0^1 j_P \psi_k(t) \int_0^1 j_Q \psi_j(s) \frac{\partial^3 G}{\partial x_p^2 \partial \mathbf{n}}(t, s, \varepsilon) ds dt &= \int_0^{\pi/4} \int_0^{\sec(\theta)} \mathcal{F}_{kj}(\rho, \theta, \varepsilon) \rho d\rho d\theta \\ &+ \int_{\pi/4}^{\pi/2} \int_0^{\csc(\theta)} \mathcal{F}_{kj}(\rho, \theta, \varepsilon) \rho d\rho d\theta \end{aligned} \tag{18}$$

Here  $j_P$  and  $j_Q$  are the (constant) jacobians for the two elements, the distance function is now

$$r^2 = \varepsilon^2 + 2b\varepsilon\rho + c^2\rho^2 \tag{19}$$

and

$$\begin{aligned}
 c^2 &= c_x^2 + c_y^2 \\
 c_x &= (x_0 - x_1) \cos(\theta) + (x_1 - x_2) \sin(\theta) \\
 c_y &= (y_0 - y_1) \cos(\theta) + (y_1 - y_2) \sin(\theta) \\
 b &= c_x N_x + c_y N_y
 \end{aligned}
 \tag{20}$$

In the last equation,  $\mathbf{N} = (N_x, N_y)$  is the (constant) unit normal on  $E_P$ .

The integration with respect to  $\rho$  produces functions  $\mathcal{F}_{kj}(\theta)$  that are finite and non-singular at  $\varepsilon=0$ , plus a divergent term for  $k=1, j=2$  of the form  $\mathcal{F}_{12}^s(\theta)/\varepsilon$ . These functions of  $\theta$  are rather lengthy expressions which need not be given here. It is of course necessary to show that the divergent term cancels with that found in Equation (13), but first we complete the discussion of the finite terms from the adjacent integral by showing that they can be integrated analytically with respect to  $\theta$ .

The functions  $\mathcal{F}_{kj}(\theta)$  are not singular, and could be integrated numerically. Although the analytic integration is sought primarily to reduce computation time, it will also replace fairly complicated expressions with simple ones and possibly improve accuracy. Moreover, for the corner discussion in Section 4, it will be useful to eliminate this numerical quadrature as a possible source of error. As the contributions from the upper limits on the  $\rho$  integration in Equation (18) disappear in the limit  $\varepsilon \rightarrow 0$ , the  $\theta$  integral is of the form

$$\int_0^{\pi/2} \mathcal{F}_{kj}(\theta) \, d\theta = \phi(Q_j) \int_0^{\pi/2} \frac{p_{kj}(\cos(\theta), \sin(\theta))}{c^6(c^2 - b^2)^{3/2}} \, d\theta
 \tag{21}$$

where  $p_{kj}$  is a polynomial and  $c$  and  $b$  are given in Equation (20). The analytic evaluation of this integral may be technically possible: a substitution of  $q = \tan(\theta)$  results in an integral over  $[0, \infty]$  of a function that is rational, except for the  $\frac{3}{2}$  power in the denominator. Nevertheless, even if feasible, this approach would lead to a lengthy expression, and thus it is better to first simplify the integrand.

The first step is to note that a translation of the co-ordinate system, namely moving  $P_1$  to the origin, does not affect the value of the derivatives. Thus, it can be assumed that  $x_1 = y_1 = 0$ , the remaining co-ordinates being shifted appropriately. Next, the co-ordinate system is rotated so that  $E_P$  becomes aligned with the positive  $x$ -axis, i.e.  $y_2 = 0, x_2 > 0, N_x = 0, N_y = -1$ . With  $(x_2, y_2)$  being the shifted co-ordinates of  $P_2$ , the rotation angle  $\Psi$  can be defined via

$$\begin{aligned}
 \cos(\Psi) &= \frac{x_2}{x_2^2 + y_2^2} \\
 \sin(\Psi) &= \frac{y_2}{x_2^2 + y_2^2}
 \end{aligned}
 \tag{22}$$

as only these quantities are required in the calculation. Unlike the translation, the rotation obviously does have an effect, the second-order derivatives being computed are now with respect to this new co-ordinate system. However, this is easy to account for through simple change of variables formulas for the derivatives.

In this new co-ordinate system Equation (21) simplifies significantly, in that the term to the  $\frac{3}{2}$  power in the denominator goes away. For example, with the change of variables  $q = \tan(\theta)$ , the integrand for the most singular term,  $k = 1, j = 2$ , becomes

$$-\frac{x_2(q+1)(x_2q-x_0)^5(x_0q^3x_2^3-3x_2q(y_0^2+x_0^2)(x_2q-x_0)+y_0^4-x_0^4)}{(x_0^2+y_0^2-2x_0x_2q+x_2^2q^2)^3((qx_2-x_0)^2)^{5/2}} \tag{23}$$

If  $x_0 < 0$ , as would be the case for a smooth surface, then this simplifies further to

$$-\frac{x_2(q+1)(x_0q^3x_2^3-3x_2q(y_0^2+x_0^2)(x_2q-x_0)+y_0^4-x_0^4)}{(x_0^2+y_0^2-2x_0x_2q+x_2^2q^2)^3} \tag{24}$$

and integrating  $q$  produces the simple result

$$\phi(Q_2) \int_0^{\pi/2} \mathcal{F}_{12}^\theta(\theta) d\theta = \frac{(x_0^2-x_0x_2+y_0^2)}{2x_2(x_0^2+y_0^2)} \phi(Q_2) \tag{25}$$

If  $P_1$  is a boundary corner with interior angle less than  $\pi/2$ , or a re-entrant corner with angle greater than  $3\pi/2$ , then  $x_0$  will be positive. Thus  $(x_2q-x_0)$  will be negative for  $0 < q \leq x_0/x_2$ , and this produces a change of sign in the integrand over this interval. The modifications required in this case are obvious.

For the reverse pair  $[P, Q]$ ,  $E_P = [P_0, P_1]$ ,  $E_Q = [P_1, P_2]$ , the co-ordinate transformation will once again place the origin at the common point  $P_1$ . In this case however, it is convenient to rotate  $E_P$  to the negative  $x$ -axis ( $x_0 < 0$ ), the rotation angle defined by

$$\begin{aligned} \cos(\Psi) &= -\frac{x_0}{x_0^2+y_0^2} \\ \sin(\Psi) &= -\frac{y_0}{x_0^2+y_0^2} \end{aligned} \tag{26}$$

these being the co-ordinates of  $P_0$  after the translation of  $P_1$  to the origin. All calculations can then proceed as for  $[Q, P]$ .

### 3.3. Cancellation

As in Reference [16], the cancellation of the  $\varepsilon^{-1}$  divergent terms follows from a direct calculation of

$$\frac{1}{\varepsilon} \int_0^{\pi/2} \mathcal{F}_{12}^s(\theta) d\theta \tag{27}$$

and comparison with Equation (13). The general expression for this integral for arbitrary  $\{P_0, P_1, P_2\}$  is, as with the finite term, quite lengthy. However, the change of co-ordinate system employed above can be invoked once again, and the integral is then manageable. In this case however, there is no need to transform the results back to the original co-ordinate system, it is sufficient to show that integrals are finite in the transformed system. The details are straightforward, and consequently omitted.

To conclude this section, we note that the above co-ordinate transformation, vital for the analytic integration and the proof of cancellation, is applicable in three dimensions, and likely to be equally useful. The corresponding situation in three dimensions is the edge-adjacent case, wherein  $E_P$  and  $E_Q$  share a common edge. Analogous to the above, it is possible to transform (the linear)  $E_P$  to the  $\{x, y\}$  plane, with the common edge forming part of the positive  $x$ -axis. It is anticipated that this will sufficiently simplify the three-dimensional expressions that the necessary analytic integrations can be carried out.

#### 4. TEST CALCULATIONS

The numerical results in this section will confirm that second-order derivatives can be accurately computed with a  $\mathcal{C}^0$  interpolation, but only for a smooth surface. The test calculations will also demonstrate that the failure at a boundary corner is due to the linear interpolation of the potential in the supersingular integral.

In the following examples, the boundary value problems are first solved using the (exterior limit) boundary integral equation for surface potential,

$$0 = \int_{\Gamma} \left( \frac{\partial \phi}{\partial \mathbf{n}}(Q)G(P, Q) - \phi(Q)\frac{\partial G}{\partial \mathbf{n}}(P, Q) \right) d\Gamma_Q \quad (28)$$

The solution of this equation, accomplished using a Galerkin approximation and a linear interpolation, completes the knowledge of the boundary potential and flux. These functions are then input into the algorithm described above for evaluating the second derivatives.

##### 4.1. Smooth surface

The first tests are Dirichlet problems on the unit disk, the boundary discretized with  $M$  uniform elements,  $M$  taking on various values. Three different boundary conditions were tested,  $\phi = x^2 - y^2$ , for which the unknown flux is exactly approximated by the linear interpolation, and  $\phi = x^3 - 3xy^2$  and  $\phi = x^4 - 6x^2y^2 + y^4$ , for which the flux and second derivatives vary more strongly with the co-ordinates. In these latter two cases therefore, the input into second derivative algorithm will be less accurate. The pointwise  $\mathcal{L}^2$  errors

$$\left[ \frac{1}{N} \sum_{j=1}^N (f_c(n_j) - f_x(n_j))^2 \right]^{1/2} \quad (29)$$

$f_c$  and  $f_x$  the computed and exact values at the nodes  $n_j$ , are listed in Tables I–III, respectively. For comparison purposes, the  $\mathcal{L}^2$  errors in the initial boundary integral solution for the surface flux are also given. Due to the symmetry, and from the Laplace equation  $\phi_{yy} = -\phi_{xx}$  (the subscripts denoting partial derivative), the errors for the derivative  $\phi_{yy}$  have to be identical to  $\phi_{xx}$ , so these numbers are omitted. In all cases, the convergence of the derivative values is roughly quadratic in  $M$  (equivalently, the mesh size), with, as expected, the results being successively less accurate as the order of the polynomial boundary data increases. The quadratic convergence is indicated in Table I by also listing the value of

$$\gamma = \frac{\log(e_k/e_{k+1})}{\log(N_k/N_{k+1})} \quad (30)$$

Table I.  $\mathcal{L}^2$  errors in the computed second derivatives for the Dirichlet problem  $\phi = x^2 - y^2$  on the unit circle.

Elements	$\partial\phi/\partial\mathbf{n}$	$\phi_{xx}$	$\phi_{xy}$	$\gamma$
50	8.735E-04	2.945E-02	2.897E-02	—
100	2.257E-04	7.172E-03	7.049E-03	1.95
150	1.014E-04	3.171E-03	3.117E-03	1.97
200	5.730E-05	1.781E-03	1.750E-03	1.98
250	3.678E-05	1.139E-03	1.119E-03	1.99
500	9.259E-06	2.958E-04	2.850E-04	1.99

Table II.  $\mathcal{L}^2$  errors in the computed second derivatives for the Dirichlet problem  $\phi = x^3 - 3xy^2$  on the unit circle.

Elements	$\partial\phi/\partial\mathbf{n}$	$\phi_{xx}$	$\phi_{xy}$
50	1.157E-03	1.099E-01	1.099E-01
100	3.190E-04	2.645E-02	2.645E-02
150	1.462E-04	1.167E-02	1.167E-02
200	8.346E-05	6.546E-03	6.546E-03
250	5.389E-05	4.184E-03	4.184E-03
500	1.372E-05	1.050E-03	1.053E-03

Table III.  $\mathcal{L}^2$  errors in the computed second derivatives for the Dirichlet problem  $\phi = x^4 - 6x^2y^2 + y^4$  on the unit circle.

Elements	$\partial\phi/\partial\mathbf{n}$	$\phi_{xx}$	$\phi_{xy}$
50	1.289E-03	2.919E-01	2.919E-01
100	3.895E-04	6.933E-02	6.933E-02
150	1.838E-04	3.051E-02	3.051E-02
200	1.065E-04	1.710E-02	1.710E-02
250	6.938E-05	1.092E-02	1.092E-02
500	1.798E-05	2.727E-03	2.707E-03

where  $N_k$  and  $e_k$  are, respectively, the number of elements and the errors. For quadratic convergence this number should be approximately equal to 2.

The second point to note is that while accurate second derivatives are obtained, and the convergence is quadratic, these values are markedly less accurate than the initial flux solution, or the post-processed gradient. As the flux is a first derivative, it is not surprising that the gradient can be calculated without loss of accuracy, and it is also to be expected that there would be a loss of accuracy in going to second derivatives.

It is worthwhile checking that accurate solutions do not depend upon the uniform grids employed in the above tests. Table IV therefore presents the errors for the quartic boundary conditions applied on the boundary of the ellipse  $x^2 + 4y^2 = 1$ . In this case the nodal points on the boundary were defined by equal increments in the central angle, thereby creating a coarser mesh near  $x = \pm 1$ . The results are roughly comparable to the corresponding values for the disk, Table III. Figure 3

## SECOND-ORDER DERIVATIVES

Table IV.  $\mathcal{L}^2$  errors in the computed second derivatives for the Dirichlet problem  $\phi = x^4 - 6x^2y^2 + y^4$  on the ellipse  $x^2 + 4y^2 = 1$ . The mesh is non-uniform.

Elements	$\partial\phi/\partial\mathbf{n}$	$\phi_{xx}$	$\phi_{xy}$
60	6.296E-03	2.650E-01	2.705E-01
100	2.279E-03	8.869E-02	9.017E-02
150	1.016E-03	3.854E-02	3.914E-02
200	5.721E-04	2.151E-02	2.183E-02
300	2.546E-04	9.505E-03	9.642E-03
600	6.377E-05	2.413E-03	2.411E-03

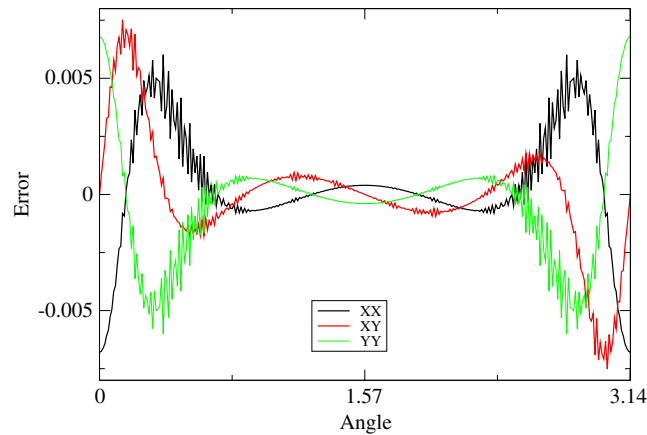


Figure 3. Nodal errors for the three second derivatives on the ellipse,  $\phi = x^4 - 6x^2y^2 + y^4$ .

plots the pointwise error as a function of angle around the top half of the ellipse, discretized with 600 nodes, the end points being the areas of poorest approximation.

In the above tests, the coefficient function of the more difficult kernel, the supersingular, was known exactly from the boundary conditions. It is therefore necessary to examine the errors when the potential function input to the derivative calculation is obtained from the boundary integral solution, and therefore contains errors. Thus, as a final example, error results are presented in Table V for a Neumann problem on an infinite domain, the exterior of ellipse employed above. Again for comparison, the  $\mathcal{L}^2$  errors for the computed potential are also given. The Neumann data

$$\frac{\partial\phi}{\partial\mathbf{n}} = n_x \frac{y^2 - x^2}{(x^2 + y^2)^2} - n_y \frac{2xy}{(x^2 + y^2)^2} \quad (31)$$

is the flux obtained from the potential function  $\phi = x/(x^2 + y^2)$ , which is the derivative of the Green's function with respect to  $x_Q$ , and the source point located at the origin. The exact derivative

Table V.  $\mathcal{L}^2$  errors in the computed second derivatives for the exterior Neumann problem on the ellipse  $x^2 + 4y^2 = 1$ .

Elements	$\phi$	$\phi_{xx}$	$\phi_{xy}$
60	1.189E-03	1.848E-01	8.019E-02
100	4.271E-04	6.670E-02	2.982E-02
150	1.896E-04	2.964E-02	1.337E-02
200	1.065E-04	1.667E-02	7.539E-03
300	4.731E-05	7.409E-03	3.358E-03
600	1.182E-05	1.859E-03	8.720E-04

solution is

$$\begin{aligned}\frac{\partial^2}{\partial^2 x} \phi &= \frac{2x^3 - 6xy^2}{(x^2 + y^2)^3} \\ \frac{\partial^2}{\partial x \partial y} \phi &= \frac{6x^2 y - 2y^3}{(x^2 + y^2)^3}\end{aligned}\tag{32}$$

and  $\phi_{yy} = -\phi_{xx}$ . Despite the errors in the potential, the accuracy is consistent with previous Dirichlet calculations, and the convergence is again roughly quadratic.

#### 4.2. Corners

The results in the previous section indicate that the limit analysis is correct, and that a  $\mathcal{C}^0$  linear interpolation provides accurate second-order derivatives, at least on a smooth surface. The same algorithm, however, applied to the unit square (lower left corner at the origin), produced highly unsatisfactory results near the boundary corners. (Away from the corners the derivatives are quite accurate, the error being less than  $1.0E - 5$  or  $1.0E - 11$  depending upon the side of the square). For this geometry, two different boundary conditions at the corners were examined, the first having mixed boundary data,  $\phi = x^2 - y^2$  on the horizontal sides of the square, and the corresponding fluxes 0 and 2 on  $x=0$  and 1. In the second, Dirichlet data with this quadratic function was employed. In each case, two different uniform meshes were employed, one with a element length of  $h = 0.0204$ , and the second  $h = 0.0101$ . Tables VI and VII list the errors near the corner  $(0, 0)$ , the results at the other three corners were similar. The errors for the Dirichlet problem were identical on either side of the corner, and thus only one side is given.

Although the second derivative errors are sensitive to the errors in the boundary integral solution at the corner (as can be seen by comparing the two tables), the failure is not due to this initial solution: even when the input to the second derivative calculation was the exact solution (instead of the boundary integral solution), the large errors remained. Note that for these two problems, no error is introduced by the linear interpolation of the geometry or surface flux, and all integrals are computed analytically. Moreover, the coefficient matrix for solving for the derivatives is well conditioned, and thus any error introduced by the linear algebra is insignificant. Thus, eliminating the error from the boundary integral solution leaves solely the linear interpolation of the quadratic potential as the source of error. Note too that the error remains consistent (as a function of mesh size) as the mesh is refined, indicating that this is in fact the answer that the linear interpolation of the potential can provide.

SECOND-ORDER DERIVATIVES

Table VI. Errors in the second derivatives near the corner (0, 0) for the mixed problem with exact solution  $\phi = x^2 - y^2$  on the unit square.

Node	$h = 0.0204$		$h = 0.0101$	
	$\phi_{xx}$	$\phi_{xy}$	$\phi_{xx}$	$\phi_{xy}$
(0, 4h)	0.096	0.002	0.096	0.002
(0, 3h)	-0.278	-0.008	-0.278	-0.008
(0, 2h)	0.760	0.029	0.760	0.029
(0, h)	-1.746	-0.109	-1.746	-0.109
(0, 0)	2.587	0.407	2.587	0.407
(h, 0)	-0.693	-0.254	-0.693	-0.254
(2h, 0)	0.186	0.098	0.186	0.098
(3h, 0)	-0.050	-0.029	-0.050	-0.029
(4h, 0)	0.013	0.012	0.013	0.012

Table VII. Errors in the second derivatives near the corner (0, 0) for the Dirichlet problem  $\phi = x^2 - y^2$  on the unit square.

Node	$h = 0.0204$		$h = 0.0101$	
	$\phi_{xx}$	$\phi_{xy}$	$\phi_{xx}$	$\phi_{xy}$
(0, 0)	4.056	-0.000	4.056	0.000
(0, h)	-1.087	-0.963	-1.087	-0.963
(0, 2h)	0.291	0.276	0.291	0.276
(0, 3h)	-0.078	-0.146	-0.078	-0.146
(0, 4h)	0.021	0.033	0.021	0.033
(0, 5h)	-0.006	-0.025	-0.006	-0.025

Additional numerical evidence that the problem is in the linear interpolation can be obtained by once again solving a problem on the unit square, only this time with the boundary conditions  $\phi = x + y$  or  $\phi = xy$ . In both cases, the linear interpolation of potential on the sides of the square is exact, and the corner second derivatives (namely zero) were indeed quite accurate. Further confirmation is seen by solving the second problem  $\phi = xy$  on the right triangle having vertices (0, 0), (1, 0) and (0, 1). The potential function on the hypotenuse is now no longer linear, and the derivative values at (1, 0) and (0, 1) were once again highly inaccurate.

This is a somewhat unusual state of affairs, in that the second derivative integral equation is mathematically well defined, and yet refining the grid will not improve the corner solution. The errors are clearly confined to the same number of nodes near the corner, independent of the mesh size  $h$ , and thus to a smaller area. This however is of little consolation if one needs accurate corner derivative values.

Nevertheless, this result is not too surprising: there is a limited amount of information that can be gleaned from the coincident and adjacent singular integrals, and thus the ability to calculate higher order derivatives must stop somewhere. For a  $\mathcal{C}^0$  interpolation, this stopping point is evidently corner values of second-order derivatives.

Note that the corresponding linear element gradient analysis does not have difficulties at boundary corners [14]. The potential in this case multiplies the hypersingular kernel, and the contributions

to the gradient from this integral must therefore only depend upon the values for the potential. It is apparent however that the supersingular kernel is dependent upon the derivative of the potential at the singular point. A hand waving argument to this effect is that if one were to integrate by parts [30–32], the supersingular integral would become hypersingular, multiplied by the derivative of  $\phi$ . Thus, while employing a higher order continuous interpolation (e.g. quadratic) may aid the corner solution, it seems more reasonable that computing accurate second-order derivatives at non-smooth boundary points will require a  $\mathcal{C}^1$  interpolation.

## 5. CONCLUSIONS

Despite the presence of ‘supersingular’ kernel functions, third-order derivatives of the Green’s function, second-order derivatives of the boundary potential can be computed directly from the boundary integral representation. This direct limit method should extend directly to other two-dimensional formulations, e.g. elasticity. Regarding extensions to three dimensions, it is expected that the limit analysis will follow along similar lines: the coincident and adjacent edge integrals will be divergent, of the form  $\varepsilon^{-1}$ , while the complete integral will be finite. However, what remains to be investigated is how much of the four dimensional parameter space integral can be evaluated analytically. In addition, the supersingular integral may now be sufficiently singular that the adjacent vertex singular integrals, which vanish for gradient evaluation, need to be considered.

A key aspect of the limit analysis is that the existence of the integrals (through cancellation of the divergent terms) requires only a  $\mathcal{C}^0$  interpolation of the potential, as compared to  $\mathcal{C}^2$  in previous work [19]. Nevertheless, accurate corner values cannot be obtained with a linear interpolation, and a  $\mathcal{C}^1$  interpolation is likely necessary for a valid corner evaluation. It is also likely that a  $\mathcal{C}^1$  interpolation will also improve the accuracy at smooth boundary points, putting it on par with that of the initial boundary integral solution.

With the limit differenced gradient algorithm, a  $\mathcal{C}^1$  interpolation in two dimensions is not difficult to arrange, a cubic Hermite approximation can be easily constructed [14, 25]. The evaluation of second-order derivatives using this approximation is currently being pursued, as is the extension to three dimensions. Note that this process, namely incorporating computed gradient values into the approximation so as to permit the evaluation of second-order derivatives, is in a way reminiscent of the bootstrapping procedure in Reference [23].

It is hoped that the ability to calculate higher order derivatives, relatively simply and accurately, will prove useful for applications such as shape optimization, contact analysis, and moving boundary problems.

## APPENDIX A

$$\frac{\partial^2 G}{\partial x \partial x} = -\frac{1}{2\pi} \left[ \frac{1}{r^2} - 2 \frac{(qx - px)^2}{r^4} \right] \quad (\text{A1})$$

$$\frac{\partial^2 G}{\partial x \partial y} = -\frac{1}{2\pi} \left[ -2 \frac{(qx - px)(qy - py)}{r^4} \right] \quad (\text{A2})$$

## SECOND-ORDER DERIVATIVES

$$\frac{\partial^3 G}{\partial \mathcal{X} \partial \mathcal{X} \partial \mathbf{n}} = -\frac{1}{2\pi} \left[ -6 \frac{n_x(q_x - p_x)}{r^4} - 2 \frac{n_x(q_y - p_y)}{r^4} + 8 \frac{\mathbf{n} \cdot \mathbf{R}(q_x - p_x)^2}{r^6} \right] \quad (\text{A3})$$

$$\frac{\partial^3 G}{\partial \mathcal{X} \partial \mathcal{Y} \partial \mathbf{n}} = -\frac{1}{2\pi} \left[ -2 \frac{\mathbf{n} \cdot \mathbf{R}}{r^4} + 8 \frac{\mathbf{n} \cdot \mathbf{R}(q_x - p_x)(q_y - p_y)}{r^6} \right] \quad (\text{A4})$$

## ACKNOWLEDGEMENTS

This research was supported in part by the Applied Mathematical Sciences Research Program of the Office of Mathematical, Information, and Computational Sciences, U.S. Department of Energy, under contract DE-AC05-00OR22725 with UT-Battelle, LLC. M. Moore acknowledges the support from the DOE Higher Education Research Experience Program at Oak Ridge National Laboratory. LJG was also supported by the Spanish Ministry of Education, Culture and Sport through the project SAB 2003-0088, and would like to thank Prof. F. Paris for the hospitality at the Department of Elasticity and Strength of Materials, Escuela Superior de Ingenieros, University of Seville.

The submitted manuscript has been authored by a contractor of the U.S. Government under contract DE-AC05-00OR22725. Accordingly the U.S. Government retains a non-exclusive, royalty free license to publish or reproduce the published form of this contribution, or allow others to do so, for U.S. Government purposes.

## REFERENCES

1. Bonnet M. *Boundary Integral Equation Methods for Solids and Fluids*. Wiley: England, 1995.
2. Paris F, Cañas J. *Boundary Element Method: Fundamentals and Applications*. Oxford University Press: Oxford, 1997.
3. Martin PA, Rizzo FJ. Hypersingular integrals: how smooth must the density be? *International Journal for Numerical Methods in Engineering* 1996; **39**:687–704.
4. Martin PA, Rizzo FJ, Cruse TA. Smoothness-relaxation strategies for singular and hypersingular integral equations. *International Journal for Numerical Methods in Engineering* 1998; **42**:885–906.
5. Gray LJ, Phan A-V, Kaplan T. Boundary integral evaluation of surface derivatives. *SIAM Journal on Scientific Computing* 2004; **26**:294–312.
6. Guiggiani M. Hypersingular formulation for boundary stress evaluation. *Engineering Analysis with Boundary Elements* 1994; **13**:169–179.
7. Wilde AJ, Aliabadi MH. Direct evaluation of boundary stresses in the 3D BEM of elastostatics. *Communications in Numerical Methods in Engineering* 1998; **14**:505–517.
8. Chati MK, Mukherjee S. Evaluation of gradients on the boundary using fully regularized hypersingular boundary integral equations. *Acta Mechanica* 1999; **135**:41–45.
9. Okada H, Rajiyah H, Atluri SN. A novel displacement gradient boundary element method for elastic stress analysis with high accuracy. *Transactions of the ASME* 1988; **55**:786–794.
10. Mantič V, Graciani E, Paris F. Potential gradient recovery using a local smoothing procedure in the Cauchy integral. *Communications in Numerical Methods in Engineering* 1999; **15**:547–556.
11. Mantič V, Graciani E, Paris F. A simple local smoothing scheme in strongly singular boundary integral representation of potential gradient. *Computer Methods in Applied Mechanics and Engineering* 1999; **178**: 267–289.
12. Graciani E, Mantič V, Paris F, Cañas J. A critical study of hypersingular and strongly singular boundary integral representations of potential gradient. *Computational Mechanics* 2000; **25**:542–559.
13. Zhao ZY, Lan S. Boundary stress calculation—a comparison study. *Computers and Structures* 1999; **71**:77–85.
14. Gray LJ, Garzon M, Mantič V, Graciani E. Galerkin boundary integral analysis for the axisymmetric Laplace equation. *International Journal for Numerical Methods in Engineering* 2006; **66**:2014–2034.

15. Gray LJ. Evaluation of singular and hypersingular Galerkin boundary integrals: direct limits and symbolic computation. In *Singular Integrals in the Boundary Element Method* (Chapter 2), Sladek V, Sladek J (eds). Advances in Boundary Elements. Computational Mechanics Publishers: Southampton, 1998; 33–84.
16. Gray LJ, Glaeser J, Kaplan T. Direct evaluation of hypersingular Galerkin surface integrals. *SIAM Journal on Scientific Computing* 2004; **25**:1534–1556.
17. Karami G, Derakhshan D. An efficient method to evaluate hypersingular and supersingular integrals in boundary integral equations analysis. *Engineering Analysis with Boundary Elements* 1999; **23**:317–326.
18. Frangi A, Bonnet M. A Galerkin symmetric and direct BIE method for kirchoff elastic plates: formulation and implementation. *International Journal for Numerical Methods in Engineering* 1998; **41**:337–369.
19. Frangi A, Bonnet M. A direct approach for boundary integral equations with high-order singularities. *International Journal for Numerical Methods in Engineering* 2000; **49**:871–898.
20. Frangi A, Bonnet M. Singular boundary elements for the analysis of cracks in plain strain. *International Journal for Numerical Methods in Engineering* 1995; **38**:2389–2411.
21. Bonnet M, Guiggiani M. Direct evaluation of double singular integrals and new free terms in 2D (symmetric) Galerkin BEM. *Computer Methods in Applied Mechanics and Engineering* 2003; **192**:2565–2596.
22. Frangi A, Guiggiani M. Boundary element analysis of Kirchoff plates with direct evaluation of hypersingular integrals. *International Journal for Numerical Methods in Engineering* 1999; **46**:1845–1863.
23. Schwab C, Wendland WL. On the extraction technique in boundary integral equations. *Mathematics of Computation* 1999; **68**:91–122.
24. Watson JO. Hermitian cubic and singular elements for plain strain. In *Developments in Boundary Element Methods* (Chapter 1), Banerjee PK, Watson JO (eds), vol. 4. Elsevier Applied Science Publishers; London and New York, 1986; 1–28.
25. Gray LJ, Garzon M. On a Hermite boundary integral approximation. *Computers and Structures* 2005; **83**:889–894.
26. Gray LJ, Maroudas D, Enmark M. Galerkin boundary integral method for evaluating surface derivatives. *Computational Mechanics* 1998; **22**:187–193.
27. Sethian JA, Wiegmann A. Structural boundary design via level set and immersed interface methods. *Journal for Computational Physics* 2000; **163**:489–528.
28. Maiti S, Paulino GH, Geubelle PH. A novel frictionless contact formulation and implementation using the boundary element method. *International Journal for Numerical Methods in Engineering* 2002.
29. de Paula FA, Telles JCF. A comparison between point collocation and Galerkin for stiffness matrices obtained by boundary elements. *Engineering Analysis with Boundary Elements* 1989; **6**:123–128.
30. Frangi A. Regularization of boundary element formulations by the derivative transfer method. In *Singular Integrals in the Boundary Element Method* (Chapter 4), Sladek V, Sladek J (eds). Advances in Boundary Elements. Computational Mechanics Publishers: Southampton, 1998; 125–164.
31. Lutz ED. Singular and nearly singular integrals. *Ph.D. Thesis*, Cornell University, 1991.
32. Nagarajan A, Lutz ED, Mukherjee S. A novel boundary elements method for linear elasticity with no numerical integration for 2d and line integrals for 3d problems. *Journal of Applied Mechanics* 1994; **61**:264–269.